Egypt. J. Chem. **Vol. 67**, No. 2 pp. 571 - 580 (2024)

Egyptian Journal of Chemistry

http://ejchem.journals.ekb.eg/

Effect of CuO on the Molecular Structural, Optical, and Electronic Properties of Polyvinyl Pyrrolidone: Experimental and DFT Approaches

Naglaa. A. M. Shahin,[a] Reham. K. Abd El Hamid, [a] and Hend A. Ezzat,[b*]

[a]*Physics Department, Faculty of Women for Arts, Science and Education, Ain Shams University, 11757 Cairo, Egypt*

[b] *Nano Technology Unit, Space Research Lab, Solar and Space Research Department, National Research Institute of Astronomy and Geophysics (NRIAG), Helwan, 11421, Cairo, Egypt*

Abstract

Nanocomposite solutions of polyvinyl pyrrolidone (PVP) embedded with different concentrations of copper oxide (CuO) nanoparticles were prepared to study the CuO effect on a polymer matrix. The obtained solutions were then properly analyzed by Fourier transform infrared spectroscopy (FTIR) and ultraviolet-visible spectroscopy (UV-Vis). In the FTIR spectra, the primary distinguishing bands of PVP and CuO were evident. The fact that some bands' strengths dropped indicates that effective reactions were going on between the functional groups inside the PVP and CuO. An optical study revealed that when the Cu^{+2} ions grew, the film's transmittance and energy band gap shrank. These results imply that the PVP matrix loaded with CuO nanoparticles has suitable structural and optical properties, boosting its potential industrial uses, notably in optical components and devices. Moreover, due to the strong reduction of transmittance to 1%, a PVP/CuO nanocomposite sample with 1.0 wt.% CuO can be used as a blocking material for the UV, visible, and near-IR regions of the electromagnetic spectrum. Theoretical results also indicated that the HOMO/LUMO band gap decreased with CuO filler while total dipole moment (TDM) increased. These findings show how experimental and theoretical work can be combined to gain a better understanding of how molecular structures interact, revealing unexpected properties of nanostructures.

Keywords: PVP nanocomposites; CuO; FTIR; Optical properties; MESP and DFT

1. Introduction

As demonstrated briefly in numerous research papers, biodegradable polymers and their matrix-based nanocomposites are now technologically established as green chemistry materials and widely used to fabricate different electronic devices [1-3]. The preparation of a variety of polymer nanocomposite (PNC) materials, which can serve as promising dielectric and optical materials in the advancement of microelectronic and optoelectronic devices, is largely preferred using biodegradable and transparent polymers such as PVP [4-6]. PVP is nearly non-toxic, highly water soluble, and produces optically transparent films when formed using the simple solution casting method [7, 8]. The mechanical and thermal properties of the pure PVP films are modest, but the amorphous PVP film breaks easily when bent [9, 10].

Due to the regular abundance of its starting material, the ease of its preparation, the fact that it is non-toxic, and its remarkably superior electrical and optical properties, copper oxide (CuO) has been concentrated as a p-type semiconductor material with a constrained band hole [11–13]. Due to their potential uses in a variety of fields, such as electronic and optoelectronic devices such as field impact transistors,

*Corresponding author e-mail: hend_ahmed16@yahoo.; (hend.ezzat@nriag.sci.eg). (Hend A. Ezzat)
EJCHEM use only: Received date here; revised date here; accepted date here
DOI: 10.21608/ejchem.2023.213585.8024

gas sensors, electrochemical cells, solar-powered cells, and nanodevices for catalysis, CuO nanoparticles are of extraordinary interest [14-16].

In the food industry, nanoparticles are frequently used to make antibacterial foods [17]. The development of antimicrobial packaging materials made with different nanoparticles, such as CuO, is currently being researched [18]. By wrapping, brushing, dipping, or spraying nano-packaging onto a food product, a selective barrier against moisture, gases, and dissolved materials can be created. The main advancements focus on producing nanoparticles through subsequent surface processing of pre-made packaging materials [19, 20].

Semiconductor nanoparticles can shield textiles, clothing, and humans from the damaging effects of UV rays [21, 22]. This is because nanoscale materials can absorb UV-based sunlight and then transform it into scattered radiation, which effectively blocks the negative effects of UV rays. The scattering of incident light over any nanosurface can be reduced by using nanoparticles because they have a larger surface area per unit volume [23]. Thus, an increase in the density of free electrons on the surface of nanoparticles reduces the intensity of scattered light and offers the possibility of reducing UV rays [24, 25]. To increase the commercial and technological applications of PVP, we set out to control its optical properties. To achieve this goal, we combined PVP with CuO nanoparticles that had been created using the precipitation method. Additionally, a theoretical study based on density functional theory was conducted to confirm the increased reactivity of PVP with the addition of CuO [26-28].

2. Materials and methods

2.1. Chemicals

PVP (M.W. ≈ 8×105 g/mol) was acquired from Alfa Aesar Company, USA. Sigma-Aldrich was used to buy copper chloride. El Nasr Pharmaceutical Chemicals Co. in Cairo, Egypt, supplied the ethanol and sodium hydroxide.

2.2. CuO nanoparticles preparation

CuO nanoparticles were prepared following the same procedures as those used in our previous work [29]. In order to obtain a homogeneous solution, 3.4 g of copper chloride was mixed with 100 ml of distilled water (DW) at 50 °C using a magnetic stirrer. Drop by drop, aqueous sodium hydroxide solution (0.4 M NaOH in 100 ml DW) was added to the copper chloride solution while stirring continuously, and the mixture was then heated to 80 ˚C for four hours. To produce copper oxide nanoparticles, the black precipitate was washed repeatedly with DW and ethanol, dried in an oven for two hours at 80 ˚C, and then calcinated for another two hours at 500 ˚C.

2.3. PVP/CuO nanocomposite solution preparation

Samples of pure PVP and its nanocomposite were prepared using the easy technique known as solution. To prepare PVP, dissolve 2 g of PVP in 50 ml of distilled water for 15 minutes. Then, various weight percentages of CuO (0.0, 0.2, 0.5, and 1.0 wt%) were loaded onto the PVP previously prepared. These different PVP/CuO weight ratios were created using the formula $X_{PVP} + Y_{CuO}$ gm, where X_{PVP} and Y_{CuO} represent the weights in gm of PVP and CuO that were used, respectively. The samples were subjected to characterization without drying. The kilos of virgin polymers used to create these blends are listed in Table 1. These solutions were further agitated for one hour at room temperature to achieve homogeneity.

Table 1 The utilized weight percentages of PVP and CuO to prepare PVP/ CuO nanocomposite solutions with different concentrations

PVP	PVP- 0.2% CuO	PVP- 0.5% CuO	PVP- 1.0% CuO	Band Assignment
3316	3309	3336	3319	OH stretching
2132	2127	2158	2159	C-H stretching
1639	1636	1637	1638	C=O

1294	1294	1294	1294	C-N stretching, CH2 wagging
945	956	960	964	C-C bond
884	869	896	838	CH2
575	584	560	559	N-C=O
-	456	434	461	Cu-O vibration

2.4. Characterization techniques

The prepared sample's functional groups were examined at room temperature using Fourier transform-infrared spectroscopy (FT-IR Bruker vertex 70, Germany) in the spectral region of (4000-400 cm^{-1}). Ultraviolet/visible spectrophotometer (UV/Vis., V-570 UV/VIS/NIR, JASCO, Japan) was carried out to determine some optical parameters in the region between 190 and 1000 nm in wavelength at room temperature.

2.5. Calculation details

Density functional theory (DFT) at the B3LYP/6-31g(d, P) level was used to calculate model structures of PVP and PVP that interacted with CuO [30-32]. The Gaussian 09 software (Gaussian, Inc., Wallingford, CT, USA) at the Molecular Spectroscopy and Modeling Unit, National Research Centre, Cairo, Egypt [33], was used to study the electronic properties of PVP and PVP decorated with CuO. TDM, HOMO/LUMO bandgap energy, and molecular electrostatic potential (MESP) are examples of the studied electronic parameters.

3. Results and Discussion

3.1. Fourier Transform Infrared (FTIR) analysis

Figure 1 displays the FTIR spectra of pure PVP and PVP integrated with various amounts of CuO- NPs in the wavelength range of 400–4000 cm^{-1}. The principal bands and functional groups associated with PVP are seen in the IR spectra of all samples. The PVP and PVP/CuO sample assignments are discussed as presented in Table 2. The following are the assigned characteristic bands for PVP:

The FTIR spectra of PVP and PVP/CuO samples contain a hydroxyl group located at 3316 cm^{-1}, a hydrocarbon group (C-H stretching) at 2132 cm^{-1}, a carbonyl group (C=O stretching) at 1639 cm^{-1}. The asymmetric wagging mode of PVP, together with the C-N stretching mode is seen at 1294 cm^{-1}. The stretching modes of the C-C and CH_2 are attributed to the two bands that are seen at 945 cm^{-1} and 884 cm^{-1}, respectively [34, 35]. The C-N (pyridine ring) within the PVP structure is responsible for the tiny band that can be seen at 575 cm^{-1}. The Cu-O mode may be identified by the absorption band of about 456 and 436 cm^{-1} confirming that the CuO reacts with the PVP chain [36].

Table 2 FTIR band assignment of PVP and PVP/ CuO samples

PVP	PVP-0.2% CuO	PVP-0.5% CuO	PVP-1.0% CuO	Band Assignment
3316	3309	3336	3319	OH stretching
2132	2127	2158	2159	C-H stretching
1639	1636	1637	1638	C=O
1294	1294	1294	1294	C-N stretching, CH2 wagging
945	956	960	964	C-C bond
884	869	896	838	CH2
575	584	560	559	N-C=O
-	456	434	461	Cu-O vibration

3.2. Ultraviolet/visible (UV-Vis) analysis

By investigating the fundamental absorption edge in the UV range, one can gain an understanding of the optical transitions and electrical band structures of crystalline and non-crystalline materials. In a variety of applications, PVP is employed as an insulator.

In this study, we looked at how adding CuO-NPs up to 1.0 wt.% affected the absorption spectra and optical band gap of PVP. Figure 2 shows the increased absorption of PVP due to the incorporation of CuO nanoparticles. All the sample's spectra had one absorption peak nearly at 234 nm that was shifted to the higher wavelength region due to CuO-NPs addition. The electronic transitions constituting the absorption band at 234 nm, were referred to as the $n \rightarrow \pi^*$ [37]. Based on the CuO-NPs concentration, a broad absorption peak was observed at nearly 722 nm, which confirms the existence of surface plasmon resonance (SPR).

This wavelength matched the other reported values well. According to another researcher, the production of SPR at 415 nm can be used to monitor the synthesis of CuO-NPs [38]. According to

numerous observations, the SPR band of copper nanoparticles was visible between 620 and 710 nm [39]. The spherical shape of copper oxide nanoparticles may be responsible for these fluctuations in the SPR, and the size distribution has an impact on both the blue shift and the surface plasmon resonance [40]. Mie's theory predicts that the absorption spectra of spherical metal nanoparticles will only contain one SPR band [41]. For the sake of the current investigation, the synthesized CuO-NPs were assumed to be spherical, and only one SPR peak was seen.

The UV-Vis transmittance spectra of the prepared samples are displayed in Figure 3 for various materials. The transmittance of PVP and PVP/CuO nanocomposite samples increases with increasing wavelength and reaches saturation at nearly 350 nm, extending to the near IR region.

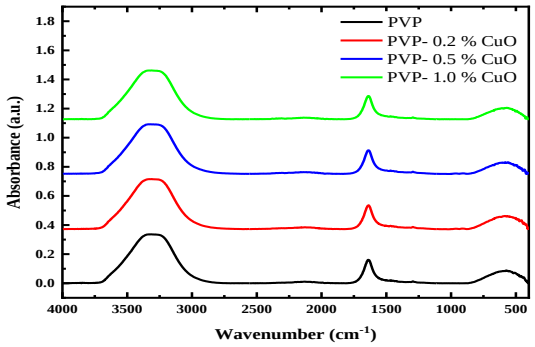

Fig. 1. The FTIR absorption spectra of PVP and PVP doped with a different weight percentage of CuO (0.2, 0.5, and 1.0 wt%).

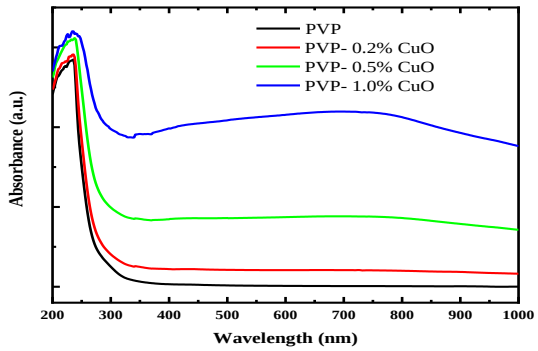

Fig. 2. UV-Vis absorption spectrum of PVP and PVP doped with different weight percentage of CuO (0.2, 0.5 and 1.0 wt%).

93% at a wavelength of 406 nm, and it steadily increases toward higher wavelengths until it reaches its maximum value of 98% at 800 nm. Transmittance drops off quickly at lower wavelengths and gets close to zero at about 250 nm. The basic absorption of light, which is brought on by the excitation of electrons from the valence band to the conduction band, is what causes the dramatic reduction toward the UV area (below 350 nm). Increasing the CuO concentration results in decreasing the transmittance of PVP until it reaches 1% for the sample containing 1.0wt.% of CuO. This confirms that it can be used as a protective layer from sunlight, as the transmittance decreased to 1% in the three spectral regions under study (UV-Vis-near IR).

The analysis of the absorption coefficient has proven to be crucial in predicting any changes to the electrical band structure of polymer materials. The optical absorption spectra can be used to identify direct and indirect transitions that have developed in the band gap of materials [42]. It is also well known that investigating the fundamental absorption edge reveals important details about the optical band gap. When an electron is excited by a photon from a lower to a higher energy state, the absorption edge is identified.

Figure 4 depicts the relationship between the absorption coefficient α and energy.

$$\alpha = 2.303 * (Abs./d) \qquad (1)$$

Where Abs. is the measured absorption and d, is the sample thickness. It was discovered that the composite has a low absorption coefficient at lower photon energy and thereafter increases at different rates reliance on the composite structure. The low absorbance coefficient of the pure sample may have been caused by its low crystallinity. The variations in the absorption edge observed for the nanocomposite samples indicate that the CuO-NPs and PVP chains interacted.

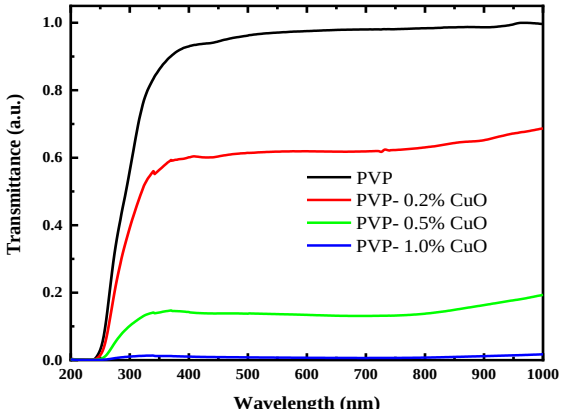

Fig. 3. Transmittance spectrum of PVP and PVP doped with different weight percentage of CuO (0.2, 0.5 and 1.0 wt%).

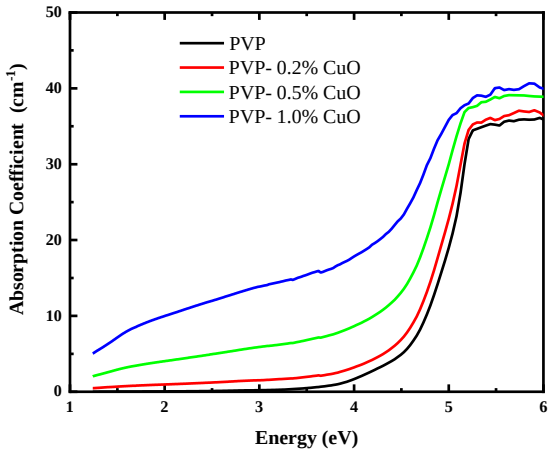

Fig. 4. Absorption coefficient of PVP and PVP doped with different weight percentage of CuO (0.2, 0.5 and 1.0 wt%) as a function of energy.

Commonly, the movement of electrons between the valence band and conduction band, which is governed by specific selection principles, is referred to as the fundamental absorption routine. It shows up as a sharp rise in the absorption region. Based on the band structure of a material, the transitions can be classified into several kinds [43]. Electronic momentum cannot be conserved throughout the transition in amorphous semiconductors with indirect band structures [44]. On the other hand, in materials with a straight band structure, momentum is preserved when the valence-to-conduction band transition occurs. The direct band gap materials' absorption coefficient is given by

$$(\alpha h\nu)=B(h\nu-E_g)^r \qquad (2)$$

Where B is a constant, Eg is the optical energy gap, and hν is the photon energy. The values of r for allowed and disallowed transitions in the direct transition are 1/2 and 3/2, respectively. For an indirect transition, r = 2 and 3, respectively, for permitted and forbidden transitions. You may calculate the band gap values by imagining the linear portions of Figures 5 and 6 along the photon energy axis. It is completely obvious that recent advancements in material quality have had a significant impact on the development of modern optoelectronic devices. Therefore, it is crucial to place the maximum emphasis on understanding a semiconductor's electrical properties, which will lead to its enormous practical importance [44]. It is wellrecognized that band structures are the source of variances in a material's electrical characteristics. As a result, understanding band gaps is crucial. The band gap values of the direct and indirect allowed transitions are shown in Table 3 for all samples. This table shows that as the CuO concentration is continuously raised, the Eg values decrease. The chemical bonds and interactions between PVP chains and CuO, which oversee producing localized states, can be linked to such a reduction in the optical energy gap. This indicates that the expansion of the localized energy levels is caused by the presence of charge transfer complexes (CTCs), which are described in terms of the rise in the degree of disorder in the samples.

The plots of ln(α) versus hν for the prepared samples are shown in Figure 7, and the Eu values, which are given in Table 3, were obtained by calculating the reciprocal of the slopes of the linear portion in the higher energy area of these curves. It is evident that as filling processes are continuously increased, Eu values rise. This causes an increase in the number of traps and a decrease in the feasibility of energy transitions, which lowers the values of Eg. According to Davis and Mott [45], the filling process caused more defect states to exist within the polymeric matrix, which is why Eu changed.

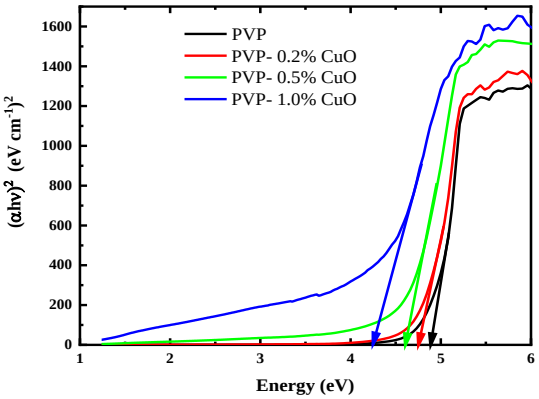

Fig. 5. Variation of $(\alpha h\nu)^2$ with photon energy for PVP and PVP doped with different weight percentage of CuO (0.2, 0.5 and 1.0 wt%).

Table 3
Direct and indirect optical bandgap values for PVP and PVP/ CuO nanocomposite samples.

PVP /x CuO-NPs	E_g^d (eV)	E_g^{in} (eV)	Eu (eV)
0	4.89	4.12	0.36
0.2	4.75	4.00	0.41
0.5	4.61	3.68	0.60
1.0	4.24	2.78	1.22

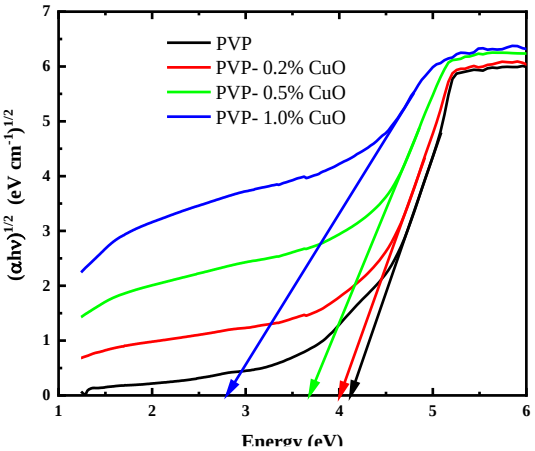

Fig. 6. Variation of $(\alpha h\nu)^{1/2}$ with photon energy for PVP and PVP doped with different weight percentage of CuO (0.2, 0.5 and 1.0 wt%).

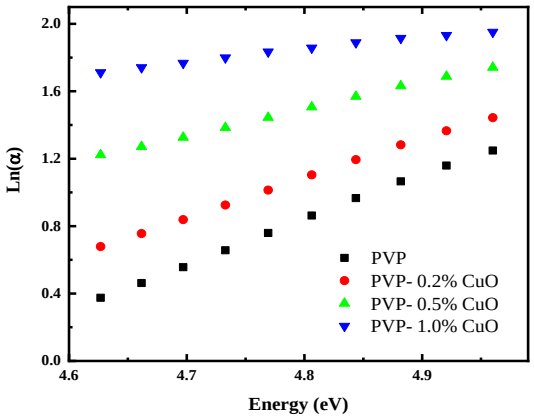

Fig. 7. Relation between lnα and hυ for PVP and PVP doped with different weight percentage of CuO (0.2, 0.5 and 1.0 wt%).

3.4. Theoretical study of PVP and PVP/CuO

DFT calculations were conducted to study the impact of nanomaterial implementation on the chemical and physical characteristics of polymers. Three PVP units were proposed to represent the polymer chain to mimic the interaction between PVP with CuO. According to the chemical structure of PVP as $(C_6H_9NO)n$ [46], three units of PVP were simulated in Figure (8-a). The most active group has an activity to interact with others, which represents the active side of interaction for PVP is the =O atom. The interaction with PVP through the =O atom is supposed to occur once through the center unit as shown in Figures (8-b and 8-c) and once through the terminal unit as shown in Figures (8-d and 8-e). Also, the CuO is proposed to interact with the PVP active side twice: once via the O atom (shown in Figures 8-b and 8-d) and once through the Cu atom (shown in Figures 8-c and 8-e). Accordingly, to study the electronic properties as well as chemical and physical property changes, TDM, bandgap energy, and MESP were investigated for PVP/CuO models.

Figure 9 illustrates the calculated HOMO-LUMO molecular orbital distribution for PVP as well as how PVP interacted with CuO in various positions. The HOMO-LUMO molecular orbitals for PVP were uniformly distributed around the three units as illustrated in Figure (9-a). According to the interaction of PVP with CuO, the orbitals are redistributed and localized around the area of interaction, which reflects the charge transfers. Table 4 also reflects the estimated TDM variation and bandgap energy (ΔE) for analyzing changes in electronic characteristics for interaction models. The TDM of PVP was recorded to be 6.515 Debye, which changed with increasing in the case of PVP/CuO Cent. and PVP/OCu Cent. to be 11.103 and 9.248 Debye, respectively. As well as, PVP TDM was changed with a decrease in the case of PVP/CuO Term. and PVP/OCu Term. to be 3.900 and 3.558 Debye, respectively. The increased TDM reflects the enhancement in electronic properties and increased structure stability. The calculated bandgap energy (ΔE) for PVP was recorded as equal to 1.768 eV. The bandgap energy (ΔE) was decreased for the different positions of interaction between PVP and CuO to be 1.413, 1.514, 1.134, and 1.077 eV for PVP/CuO Cent., PVP/OCu Cent., PVP/CuO Term., and PVP/OCu Term., respectively. The most probable model of interaction was PVP/CuO Cent., which records an increase in the TDM with a decrease in bandgap energy (ΔE) [47]. Furthermore, this structure is the most electrically enhanced and chemically stable.

The MESP is one of the many descriptors that reflect the change in the structure reactivity according to the chemical interactions. The importance of MESP came from the extracted information from the MESP color map that explains the changes in reactivity according to the charge [48]. Figure 10-a demonstrates the MESP color map of PVP, which shows the more active region around the =O atom represented by the red color (the greatest charge area), and the other

structure is neutral, represented by the yellow color. When PVP interacted with CuO in different positions, the red color intensity of the regions on the polymer chain was increased around the =O atom and CuO as shown in Figure 10. The most increased red color was for the structures PVP/CuO Cent. and PVP/OCu Term. Accordingly, the most active and electrically improved structure was PVP/CuO Cent., which matched and confirmed the TDM and band gap results.

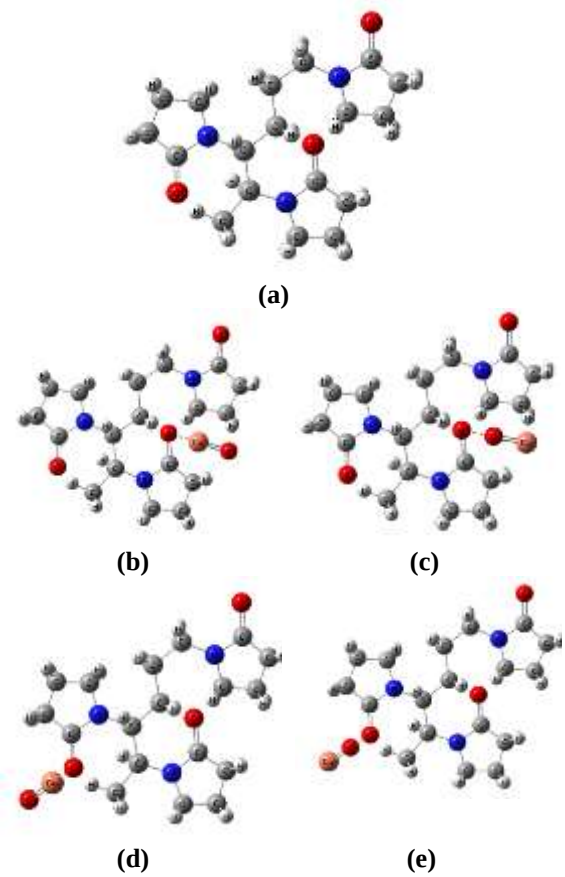

Fig. 8. Optimized structures of: a) PVP, b) PVP/CuO Cent, c) PVP/OCu Cent, d) PVP/CuO Term, and e)PVP/OCu.

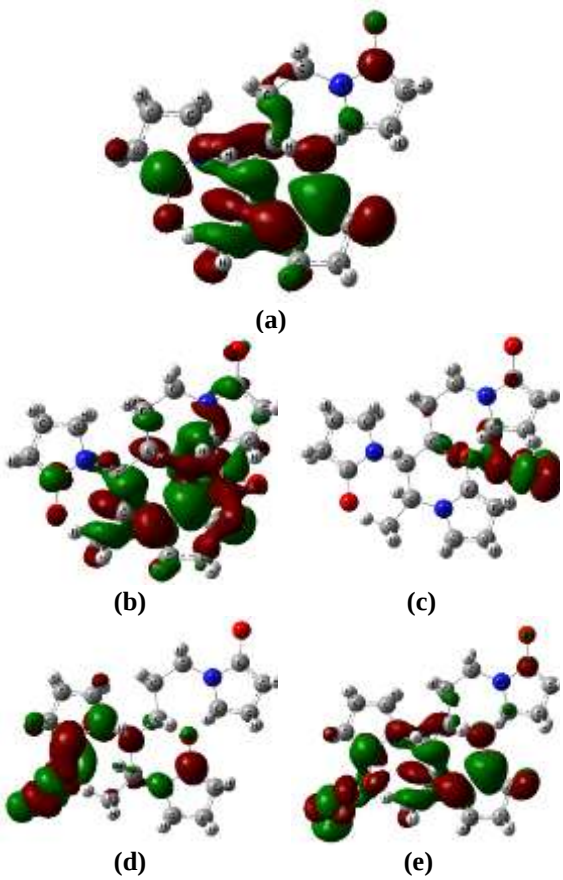

Fig. 9. B3LYP/6-31g(d,p) calculated HOMO/LUMO molecular orbitals of: a) PVP, b) PVP/CuO Cent, c) PVP/OCu Cent, d) PVP/CuO Term, and e)PVP/OCu.

Table 4

Calculated TDM (Debye) and HOMO-LUMO bandgap energy ΔE (eV) using DFT: B3LYP/6-31g(d,p) for PVP and PVP/CuO model molecules.

Structures	TDM (Debye)	ΔE (eV)
PVP	6.515	1.768
PVP/CuO Cent	11.103	1.413
PVP/OCu Cent	9.248	1.514
PVP/CuO Term	3.900	1.134
PVP/OCu Term	3.558	1.077

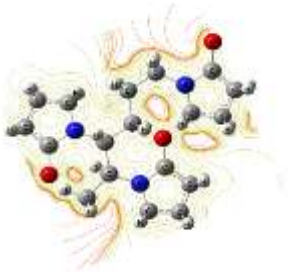

(a)

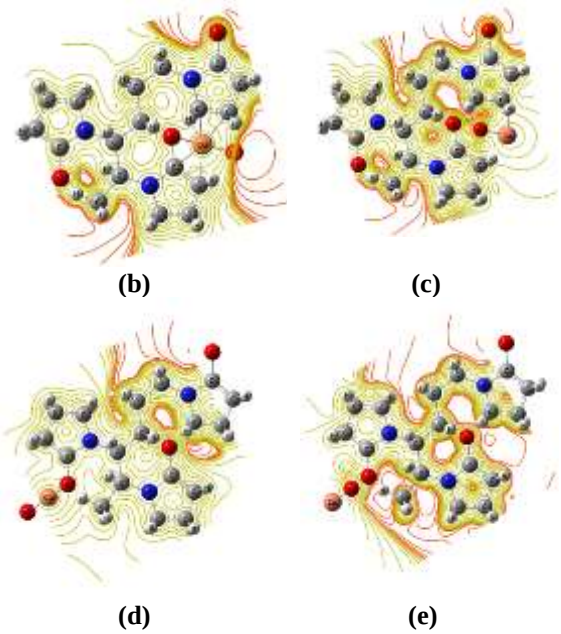

Fig. 10. B3LYP/6-31g(d,p) calculated MESP of: a) PVP, b) PVP/CuO Cent, c) PVP/OCu Cent, d) PVP/CuO Term, and e)PVP/OCu.

4. Conclusions

This work examines the optical properties of polymer nanocomposite samples based on PVP and CuO nanoparticles that have a narrow optical band gap. Using the solution casting approach, CuO nanoparticles have been incorporated into a PVP host polymer solution with different weight percentages. CuO nanoparticles and PVP nanocomposites interacted, as shown by the measurements of the FTIR spectra, through the formation of hydrogen bonding. For nanocomposite materials, a wide absorption zone was seen that almost completely covered the UV-visible to near-infrared regions. Thus, the absorption edge was shifted to the lower energy region. Moreover, it was discovered that Tauc's model was essential for identifying the different kinds of electron transfer. When PVP was doped with CuO, the optical band gap decreased from 4.89 eV to 4.24 eV and from 4.12 eV to 2.78 eV for direct and indirect transitions, respectively. As the PVP/CuO nanocomposite samples exhibit a blocking percentage of more than 98% for UV radiation, it's concluded that it can be used as a safe UV-blocking material.

5. Conflicts of interest

The authors declare that there are no conflicts with interest.

6. Formatting of funding sources

There is no received fund.

7. Acknowledgments

The authors would like to acknowledge the computational facilities at Molecular Spectroscopy and Modeling Unit, National Research Centre, Cairo, Egypt.

8. References

[1] Badry, R., El-Khodary, S., Elhaes, H., Nada, N., & Ibrahim, M. (2021). Optical, conductivity and dielectric properties of plasticized solid polymer electrolytes based on blends of sodium carboxymethyl cellulose and polyethylene oxide. Optical and Quantum Electronics, 53(1), 1-15.

[2] Badry, R., Nada, N., El-Nahass, M. M., Elhaes, H., & Ibrahim, M. A. (2022). The Detection of NH3, H2S and HBr Gases by Carboxymethyl Cellulose Sodium/ZnO Nanocomposites: A Theoretical Study. Egyptian Journal of Chemistry, 65(7), 281-292.

[3] Ezzat, H. A., Hegazy, M. A., Nada, N. A., Osman, O., & Ibrahim, M. A. (2023). Studying the optical and thermal properties of Cs/ZnO and Cs/ZnO/GO hybrid nanocomposites. Optical Materials, 135, 113244.

[4] Dhatarwal, P., & Sengwa, R. J. (2021). Investigation on the optical properties of (PVP/PVA)/Al2O3 nanocomposite films for green disposable optoelectronics. Physica B: Condensed Matter, 613, 412989.

[5] Deeba, F., Bafna, M., & Jain, A. (2021). Tuning of electrical properties of polymer blends or composites by doping of salts and inorganic fillers: A review. SGVU Int. J. Environ. Sci. Technol, 8, 46.

[6] Ragab, H. M. (2022). Enhancement in optical, thermal and electrical properties of Polyvinyl pyrrolidone/polyethylene oxide matrix-based nanocomposites for advanced flexible optoelectronic technologies considering nanoceramic zinc oxide/titanium dioxide filler. Journal of Molecular Structure, 134663.

[7] Kurakula, M., & Rao, G. K. (2020). Pharmaceutical assessment of polyvinylpyrrolidone (PVP): As excipient from conventional to controlled delivery systems with a spotlight on COVID-19 inhibition. Journal of Drug Delivery Science and Technology, 60, 102046.

[8] Helberg, R. M. L., Dai, Z., Ansaloni, L., & Deng, L. (2020). PVA/PVP blend polymer matrix for hosting carriers in facilitated transport membranes: Synergistic enhancement of CO2 separation performance. Green Energy & Environment, 5(1), 59-68.

[9] Kusumawati, D. H., Rohmawati, L., Uzalia, P., Layli, M. D., Rahanti, A. B., & Yuliani, I. (2022).

Effectiveness of Polyvinyl Alcohol Nanofiber Composites as Anti-Bacterial Materials in Wound Dressing. In Journal of Physics: Conference Series IOP, 2392 (1), 012018.

[10] Mohammed, M. I. (2022). Controlling the optical properties and analyzing mechanical, dielectric characteristics of MgO doped (PVA–PVP) blend by altering the doping content for multifunctional microelectronic devices.

[11] Gomaa, H. M., AlAbdulaal, T. H., Yahia, I. S., Ismail, A. M., Mohammmed, M. I., Zahran, H. Y., ... & Ibrahim, M. A. (2022). Exploring the Optical and Electrical Properties of 70% PVP/30% PVA Blend Polymer Doping with Graphene Thin Films For Optoelectronics Applications. Journal of Electronic Materials, 51(10), 5897-5907.

[12] Wang, Y., & Pierson, J. F. (2021). Binary copper oxides as photovoltaic absorbers: recent progress in materials and applications. Journal of Physics D: Applied Physics, 54(26), 263002.

[13] Wang, L., Ma, X., Huang, G., Lian, R., Huang, J., She, H., & Wang, Q. (2022). Construction of ternary CuO/CuFe2O4/g-C3N4 composite and its enhanced photocatalytic degradation of tetracycline hydrochloride with persulfate under simulated sunlight. Journal of Environmental Sciences, 112, 59-70.

[14] Zhang, J., Ma, S., Wang, B., & Pei, S. (2021). Preparation of composite SnO2/CuO nanotubes by electrospinning and excellent gas selectivity to ethanol. Sensors and Actuators A: Physical, 332, 113090.

[15] Xu, L., Zheng, G., Pei, S., & Wang, J. (2018). Investigation of optical bandgap variation and photoluminescence behavior in nanocrystalline CuO thin films. Optik, 158, 382-390.

[16] Navale, Y. H., Navale, S. T., Chougule, M. A., Ramgir, N. S., & Patil, V. B. (2021). NO_2 gas sensing properties of heterostructural CuO nanoparticles/ZnO nanorods. Journal of Materials Science: Materials in Electronics, 32(13), 18178-18191.

[17] Li, Z., Guo, L., Feng, Z., Gao, S., Zhang, H., Yang, X., and Pan, G. (2022). Metal-organic framework-derived ZnO decorated with CuO for ultra-high response and selectivity H_2S gas sensor. Sensors and Actuators B: Chemical, 366, 131995.

[18] Omerović, N., Djisalov, M., Živojević, K., Mladenović, M., Vunduk, J., Milenković, I., ... & Vidić, J. (2021). Antimicrobial nanoparticles and biodegradable polymer composites for active food packaging applications. Comprehensive Reviews in Food Science and Food Safety, 20(3), 2428-2454.

[19] Zeng, J., Ren, X., Zhu, S., & Gao, Y. (2021). Fabrication and characterization of an economical active packaging film based on chitosan incorporated with pomegranate peel. International Journal of Biological Macromolecules, 192, 1160-1168.

[20] Mustafa, F., & Andreescu, S. (2020). Nanotechnology-based approaches for food sensing and packaging applications. RSC advances, 10(33), 19309-19336.

[21] Sagar, N. A., Kumar, N., Choudhary, R., Bajpai, V. K., Cao, H., Shukla, S., & Pareek, S. (2022). Prospecting the role of nanotechnology in extending the shelf-life of fresh produce and in developing advanced packaging. Food Packaging and Shelf Life, 34, 100955.

[22] Kibria, G., Repon, M., Hossain, M., Islam, T., Jalil, M. A., Aljabri, M. D., & Rahman, M. M. (2022). UV-blocking cotton fabric design for comfortable summer wears: factors, durability and nanomaterials. Cellulose, 1-31.

[23] Huang, R., Zhang, S., Zhang, W., & Yang, X. (2021). Progress of zinc oxide-based nanocomposites in the textile industry. IET Collaborative Intelligent Manufacturing, 3(3), 281-289.

[24] Ray, P. C. (2010). Size and shape dependent second order nonlinear optical properties of nanomaterials and their application in biological and chemical sensing. Chemical reviews, 110(9), 5332-5365.

[25] Hashim, A., Al-Attiyah, K. H. H., & Obaid, S. F. (2019). Fabrication of novel (biopolymer blend-lead oxide nanoparticles) nanocomposites: structural and optical properties for low-cost nuclear radiation shielding. Ukrainian Journal of Physics, 64(2), 157-157.

[26] Yuan, H., Li, T., Wang, Y., Ma, P., Du, M., Liu, T., ... & Dong, W. (2020). Photoprotective and multifunctional polymer film with excellent near-infrared and UV shielding properties. Composites Communications, 22, 100443.

[27] Badry, R., Fahmy, A., Ibrahim, A., Elhaes, H., & Ibrahim, M. (2021). Application of polyvinyl alcohol/polypropylene/zinc oxide nanocomposites as sensor: modeling approach. Optical and Quantum Electronics, 53(1), 1-12.

[28] Refaat, A., Ibrahim, M. A., Elhaes, H., Badry, R., Ezzat, H., Yahia, I. S., ... & Shkir, M. (2019). Geometrical, vibrational and physical properties of polyvinyl chloride nanocomposites: Molecular modeling approach. Journal of Theoretical and Computational Chemistry, 18(08), 1950037.

[29] Hegazy, M. A., Ezzat, H. A., Yahia, I. S., Zahran, H. Y., Elhaes, H., Gomaa, I., & Ibrahim, M. A. (2022). Effect of CuO and graphene on PTFE microfibers: experimental and modeling approaches. Polymers, 14(6), 1069.

[30] Omar, A., Badry, R., Hegazy, M. A., Yahia, I. S., Elhaes, H., Zahran, H. Y., ... & Refaat, A. (2022). Enhancing the optical properties of chitosan, carboxymethyl cellulose, sodium alginate modified with nano metal oxide and graphene oxide. Optical and Quantum Electronics, 54(12), 1-15.

[31] Axel, D. B. (1993). Density-functional thermochemistry. III. The role of exact exchange. The Journal of chemical physics, 98(7), 5648-5652.

[32] Lee, B. S. (1992). Causal relations among stock returns, interest rates, real activity, and inflation. The Journal of Finance, 47(4), 1591-1603.

[33] Myrseth, V., Bozek, J. D., Kukk, E., Sæthre, L. J., & Thomas, T. D. (2002). Adiabatic and vertical carbon 1s ionization energies in representative small molecules. Journal of electron spectroscopy and related phenomena, 122(1), 57-63.

[34] Frisch, M. J., Trucks, G. W., Schlegel, H. B., Scuseria, G. E., Robb, M. A., Cheeseman, J. R., Scalmani, G., Barone, V., Mennucci, B., Petersson, G. A., Nakatsuji, H., Caricato, M., Li, X., Hratchian, H. P., Izmaylov, A. F., Bloino, J., Zheng, G., Sonnenberg, J. L., Hada, M., Ehara, M., Toyota, K., Fukuda, R., Hasegawa, J., Ishida, M., Nakajima, T., Honda, Y., Kitao, O., Nakai, H., Vreven, T., Montgomery Jr., J.A., Peralta, J. E., Ogliaro, F., Bearpark, M., Heyd, J. J., Brothers, E., Kudin, K. N., Staroverov, V. N., Keith, T., Kobayashi, R., Normand, J., Raghavachari, K., Rendell, A., Burant, J. C., Iyengar, S. S., Tomasi, J., Cossi, M., Rega, N., Millam, J. M., Klene, M., Knox, J. E., Cross, J. B., Bakken, V., Adamo, C., Jaramillo, J., Gomperts, R., Stratmann, R. E., Yazyev, O., Austin, A. J., Cammi, R., Pomelli, C., Ochterski, J. W., Martin, R. L., Morokuma, K., Zakrzewski, V. G., Voth, G. A., Salvador, P., Dannenberg, J. J., Dapprich, S., Daniels, A. D., Farkas, O., Foresman, J. B., Ortiz, J. V., Cioslowski, J., Fox, D. J. Gaussian 09, Revision C.01, Gaussian, Inc., Wallingford, CT, (2010).

[35] Teodorescu, M., Bercea, M., & Morariu, S. (2019). Biomaterials of PVA and PVP in medical and pharmaceutical applications: Perspectives and challenges. Biotechnology advances, 37(1), 109-131.

[36] Wang, J., Liu, W., Song, X., Ma, Y., & Huang, Y. (2018). Effects of added polyvinyl pyrrolidone on morphology and microstructure of multiple-phase mullite nanofibers. Ceramics International, 44(13), 15418-15427.

[37] Ramani, R. V., Ramani, B. M., Saparia, A. D., Dhruv, D., & Markna, J. H. (2016). Synthesis and optical characterization of CuO nanoparticles on solar borosilicate glass. In Journal of Nano Research, Trans Tech Publications Ltd. 37, 68-73.

[38] Abdelghany, A. M., Morsi, M. A., Abdelrazek, A., & Ahmed, M. T. (2018). Role of silica nanoparticles on structural, optical and morphological properties of poly (vinyl chloride-co-vinyl acetate-co-2-hydroxypropyl acrylate) copolymer. Silicon, 10(2), 519-524.

[39] Chtita, S., Larif, M., Ghamali, M., Bouachrine, M., & Lakhlifi, T. (2015). Quantitative structure–activity relationship studies of dibenzo [a, d] cycloalkenimine derivatives for non-competitive antagonists of N-methyl-d-aspartate based on density functional theory with electronic and topological descriptors. Journal of Taibah University for Science, 9(2), 143-154..

[40] Cuevas, R., Durán, N., Diez, M. C., Tortella, G. R., & Rubilar, O. (2015). Extracellular biosynthesis of copper and copper oxide nanoparticles by Stereum hirsutum, a native white-rot fungus from chilean forests. Journal of Nanomaterials, 2015.

[41] Moores, A., & Goettmann, F. (2006). The plasmon band in noble metal nanoparticles: an introduction to theory and applications. New Journal of Chemistry, 30(8), 1121-1132.

[42] Mie, G. (1908). Contribution to the optics of turbid media specifically colloidal metal particles. Annalen der Physik, 25, 377-445.

[43] Aziz, S. B., Abdullah, O. G., & Rasheed, M. A. (2017). A novel polymer composite with a small optical band gap: New approaches for photonics and optoelectronics. Journal of Applied Polymer Science, 134(21).

[44] Ahmed, N. M., Sauli, Z., Hashim, U., & Al-Douri, Y. (2009). Investigation of the absorption coefficient, refractive index, energy band gap, and film thickness for Al0. 11Ga0. 89N, Al0. 03Ga0. 97N, and GaN by optical transmission method. International Journal of Nanoelectronics and Materials, 2(189), e195.

[45] Davis, E. A., & Mott, N. (1970). Conduction in non-crystalline systems V. Conductivity, optical absorption and photoconductivity in amorphous semiconductors. Philosophical magazine, 22(179), 0903-0922.

[46] Abdelghany, A. M., Meikhail, M. S., Oraby, A. H., & Aboelwafa, M. A. (2023). Experimental and DFT studies on the structural and optical properties of chitosan/polyvinyl pyrrolidone/ZnS nanocomposites. Polymer Bulletin, 1-20.

[47] Al-Fifi, Z., Eid, M., Saleh, N. A., & Ibrahim, M. (2014). Molecular Modelling Analyses of the Substituted 3′-Azido-2′, 3′ Dideoxythymidine. Journal of Computitional and Theortical Nanoscince, 11, 409-412.

[48] Politzer, P., Laurence, P. R., & Jayasuriya, K. (1985) Molecular electrostatic potentials: an effective tool for the elucidation of biochemical phenomena. Environmental Health Perspectives, 61, well-recognized -202.